

Perturbation dynamics in unsteady pipe flows

By M. ZHAO¹, M. S. GHIDAOU²† AND A. A. KOLYSHKIN³

¹Department Engineering Mechanics, Dalian University of Technology, Dalian 116024, China

²Department of Civil Engineering, The Hong Kong University of Science and Technology, Hong Kong

³Department of Engineering Mathematics, Riga Technical University Riga, Latvia LV 1048

(Received 8 July 2005 and in revised form 10 May 2006)

This paper deals with perturbed unsteady laminar flows in a pipe. Three types of flows are considered: a flow accelerated from rest; a flow in a pipe generated by the controlled motion of a piston; and a water hammer flow where the transient is generated by the instantaneous closure of a valve. Methods of linear stability theory are used to analyse the behaviour of small perturbations in the flow. Since the base flow is unsteady, the linearized problem is formulated as an initial-value problem. This allows us to consider arbitrary initial conditions and describe both short-time and long-time evolution of the flow. The role of initial conditions on short-time transients is investigated. It is shown that the phenomenon of transient growth is not associated with a certain type of initial conditions. Perturbation dynamics is also studied for long times. In addition, optimal perturbations, i.e. initial perturbations that maximize the energy growth, are determined for all three types of flow discussed. Despite the fact that these optimal perturbations, most probably, will not occur in practice, they do provide an upper bound for energy growth and can be used as a point of reference. Results of numerical simulation are compared with previous experimental data. The comparison with data for accelerated flows shows that the instability cannot be explained by long-time asymptotics. In particular, the method of normal modes applied with the quasi-steady assumption will fail to predict the flow instability. In contrast, the transient growth mechanism may be used to explain transition since experimental transition time is found to be in the interval where the energy of perturbation experiences substantial growth. Instability of rapidly decelerated flows is found to be associated with asymptotic growth mechanism. Energy growth of perturbations is used in an attempt to explain previous experimental results. Numerical results show satisfactory agreement with the experimental features such as the wavelength of the most unstable mode and the structure of the most unstable disturbance. The validity of the quasi-steady assumption for stability studies of unsteady non-periodic laminar flows is discussed.

1. Introduction

The study of unsteady fluid flows in pipes is important for a wide range of applications such as design and analysis of water supply, natural gas and pressurized sewerage pipeline systems, analysis of transient-induced water quality problems in water supply lines, study of transient-based inverse modelling for the purposes of calibration and/or leakage detection in pipes, investigation of sloughing-off and the fate of bio-film during transient events in water and sea-water pipelines and analysis

† Author to whom correspondence should be addressed: ghidaoui@ust.hk

of blood flow in arteries. Fluid transients in water supply and natural gas pipelines can be generated by actions such as pump starts and valve opening. The steady flow of much of these applications belong to the highly turbulent regime. However, during unsteady events, the flow regime often undergoes transition from the laminar to the turbulent regime or vice versa. For example, a sudden start of the flow by, say, turning on a pump takes the flow through all stages: from laminar flow to the transition from laminar to turbulent flow and eventually to a steady-state highly turbulent flow. On the other hand, sudden flow deceleration by, say, pump failure can take the flow from the fully turbulent regime to the laminar regime. Pressures triggered by flow unsteadiness are known to cause rupture of pipelines, damage to other hydraulic devices and fire-related damage in the case of natural gas pipelines (Wylie & Streeter 1993). The pressure in unsteady flow can also acquire values low enough to cause cavitation, pitting and corrosion, and the intrusion of contaminants through cracks and joints (Brunone *et al.* 2000). Water quality in supply lines can be affected following a transient event as bio-film on the pipe is sloughed off by the large shear stresses created by the transient, and particulates may be re-suspended by the strong mixing of the flow inside a pipe. In addition, blood-flow unsteadiness can result in atherosclerosis plaque development in regions where the shear stress changes direction (Waters & Pedley 1999).

Temporal linear stability theory reveals that unsteady pipe flows are susceptible to two types of instability, namely, exponential instability and transient instability (von Kerczek 1982; Schmid & Henningson 2001). Exponential instability may occur if there is a favourable range of parameters for which one or more normal modes (travelling waves) can grow exponentially. The study of exponential growth or decay of instabilities is restricted to providing the long term behaviour (i.e. as time tends to infinity) of the most dominant mode. The transient growth instability is related to the fact that the superposition of normal modes may initially experience a large growth even when each of the modes is decaying and is due to the non-orthogonality of the eigenvectors of the linear operator and is intimately linked to the lift-up of streamwise vortices. The transient growth can be large enough to cause transition to either another laminar state or to a turbulent state, rendering the exponential stability a moot point (Criminale *et al.* 1997; Schmid & Henningson 2001); thus, the name bypass instability.

Much of the work on the linear stability of unsteady pipe flows in pipes and channels has concentrated on the investigation of the exponential instability mechanism through the use of the method of normal modes (e.g. Hall 1975; Hino, Sawamoto & Takasu 1976; Hall & Parker 1976; Yang & Yih 1977; von Kerczek 1982; Das & Arakeri 1998; Ghidaoui & Kolyshkin 2002). Such studies have determined the main parameters governing the exponential instability of time-dependent pipe flows and established the ranges of parameters where perturbations grow exponentially. The conditions under which properties of flow unsteadiness, such as amplitude and frequency for the case of oscillatory flows and flow acceleration or deceleration for the case of non-periodic flows, promote or suppress the exponential instability have been investigated. Reasonable quantitative agreement between the critical parameters associated with the exponential instability and experiments has been found, especially for problems when the base flow is rapidly decelerated and contains inflection points (Das & Arakeri 1998).

The use of the method of normal modes to investigate the susceptibility of time-dependent pipe flows to exponential instability is a natural starting point in stability theory. However, previous studies (see, for example, Schmid & Henningson 2001

and references therein) indicated that, in some cases, the method of normal modes gives only a partial description of the linear perturbation equations. In addition, the application of the method of normal mode analysis to time-dependent flows usually requires the adoption of the quasi-steady assumption.

These limitations associated with the method of normal mode analysis can be overcome by investigating the time evolution of infinitesimal perturbations as an initial-value problem. The solution of the initial-value problem provides the evolution of perturbations for all time, thus, allowing the investigation of the behaviour of disturbances during the initial transient growth phase as well as the long-term asymptotic phase. The transient growth phase is crucial for understanding (i) the behaviour of perturbations in flows that are deemed unconditionally stable by the method of normal modes such as steady pipe flow; (ii) the subcritical instability in flows that are known to experience transition in regimes where the flow is deemed stable by the method of normal modes such as steady channel flow; and (iii) the bypass transition in flows that are known to develop streaks and undergo transition well before the exponential instability has a chance to set in. The initial-value problem approach has been successfully applied to a wide range of steady-flow problems (e.g. Lasseigne *et al.* 1999; Corbett & Bottaro 2000; Schmid 2000; Schmid & Henningson 2001). Von Kerczek (1982) has shown that some time-dependent flows can also exhibit significant transient growth. In particular, he found that the transient behaviour of perturbations can cause the flow to undergo transition even though the long-term average growth of perturbations is small. Transient growth, which occurs for small values of time, may lead to the rapid instability observed in the unsteady pipe flow experiments of Lefebvre & White (1989), Brunone *et al.* (2000) and Greenblatt & Moss (2003). Note, however, that by-pass transition mechanism requires nonlinearity. The linearized stability equations describe only the initial stage of the development of instability.

The transient growth mechanism depends on the form of the initial perturbation. Various methods can be used in order to optimize the initial perturbation and obtain maximum transient growth amplification. Butler & Farrell (1992), Bergström (1993), Reddy & Henningson (1993) and Schmid & Henningson (1994) studied different aspects of the transient growth of the optimal perturbations in plane channel flow and pipe Poiseuille flow.

The present paper is devoted to the linear stability analysis of time-dependent base flows in a pipe. The flows considered are those studied experimentally by Lefebvre & White (1989) and Das & Arakeri (1998) as well as the water hammer flow (Hall & Parker 1976). The first two papers contain the data required to allow comparison between linear stability theory and experiments. The stability analysis is based on the solution of the initial-value problem obtained by linearizing the Navier–Stokes equation in the neighbourhood of the base flow and adopting a Fourier decomposition in the longitudinal and azimuthal directions. The initial-value problem provides the behaviour of perturbations for all time. The sensitivity of the time behaviour of perturbations to the initial conditions is investigated. In addition, optimal perturbations which give the upper limit of the energy growth are also computed and used as a point of reference.

The stability results are compared with the experimental findings of Lefebvre & White (1989) and Das & Arakeri (1998). It is shown that the transient growth phase is essential in explaining the transition observed in some of the experiments, especially for non-inflectional time-dependent base flows. The resolution of the time behaviour of perturbations is also instrumental in developing criteria to explain why

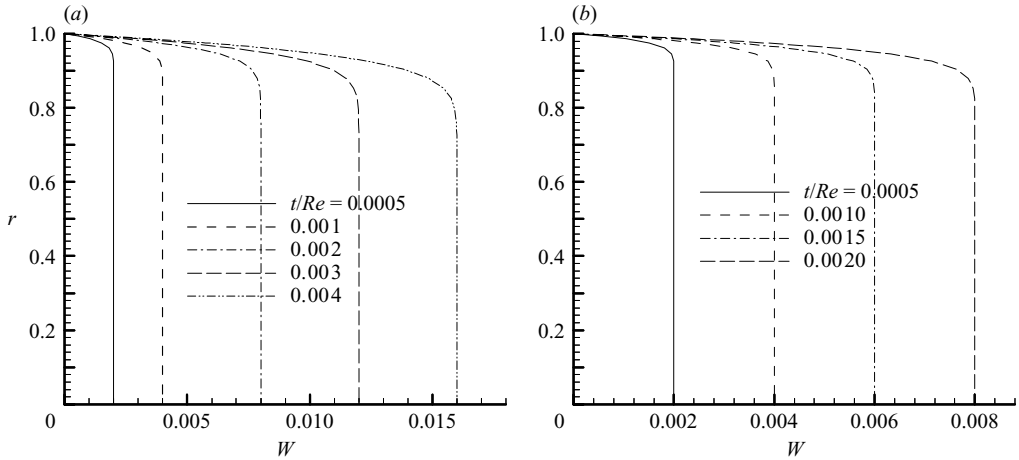


FIGURE 1. Velocity profiles for accelerated flows (Lefebvre & White 1989). (a) Case 1: the Reynolds number based on mean velocity and diameter is $Re_D = 2.4 \times 10^5$ and (b) Case 2: the Reynolds number based on mean velocity and diameter is $Re_D = 5.2 \times 10^5$.

the experiments of Das & Arakeri (1998) show that flow instability does not always lead to turbulence.

2. Formulation of the stability model

2.1. Base flows

A general axisymmetric one-dimensional flow field in a circular pipe has the following generic form,

$$\tilde{W} = \tilde{W}(\tilde{r}, \tilde{t}), \quad \tilde{P} = \tilde{P}(\tilde{z}, \tilde{t}), \quad (1)$$

where \tilde{t} is dimensional time, \tilde{z} is the dimensional axial coordinate, \tilde{r} is the dimensional radial coordinate, \tilde{W} is the dimensional flow velocity along axial direction and \tilde{P} is dimensional pressure. This base flow is the solution of the following equation (Schlichting 1979),

$$\frac{\partial \tilde{W}}{\partial \tilde{t}} = -\frac{1}{\rho} \frac{\partial \tilde{P}}{\partial \tilde{z}} + \nu \left(\frac{\partial^2 \tilde{W}}{\partial \tilde{r}^2} + \frac{1}{\tilde{r}} \frac{\partial \tilde{W}}{\partial \tilde{r}} \right), \quad (2)$$

where ρ is the density of the fluid; ν is the kinematic viscosity of the fluid.

Three types of transient flows are analysed in this paper, namely, flow accelerated from rest (Lefebvre & White 1989), unsteady flows with acceleration and deceleration phases generated by the motion of a piston (Das & Arakeri 1998) and water hammer flows (fully developed laminar flows subject to rapid deceleration). The velocity profiles in accelerated flows do not contain inflection points whereas in the cases of rapidly decelerated flows the velocity distribution has inflection points present throughout the deceleration phase.

The base flow velocity profiles for the case of flow accelerated from rest (Lefebvre & White 1989) are obtained from analytical solution given by Gromeka (1882) whose solution was later reproduced by Szymanski (1932). The velocity profiles for two selected cases (hereinafter referred to as Case 1 and Case 2) are plotted in figure 1. Case 1 defines the problem for which the Reynolds number Re based on mean velocity and diameter is 2.4×10^5 and the measured dimensionless transitional time

Case	\tilde{t}_0 (s)	\tilde{t}_1 (s)	\tilde{t}_2 (s)	\tilde{t}_p (s)	U_p (m s ⁻¹)	$Re = U_p R/\nu$
I	0.13	10.26	10.27	19.2	0.054	684
II	0.42	3.68	4.04	6.24	0.16	2036.5
III	0.14	1.86	2.46	2.76	0.33	4251
IV	0.13	0.44	1.10	1.80	0.33	4251

TABLE 1. Parameters of the experiments reported by Das & Arakeri (1998).

is $\hat{t} = t/Re = 0.0032$. Case 2 defines the problem for which the Reynolds number based on mean velocity and diameter is 5.2×10^5 and the measured dimensionless transitional time is $\hat{t} = t/Re = 0.00105$.

Das & Arakeri (1998) studied another type of transient flow. The test rig consisted of a pipe–piston system. The flow of an incompressible fluid (water) was generated as follows: the velocity of the piston linearly increases from zero to some constant velocity \tilde{U}_p for $0 < \tilde{t} < \tilde{t}_0$, maintains a constant value \tilde{U}_p for $\tilde{t}_0 < \tilde{t} < \tilde{t}_1$, linearly decreases to zero for $\tilde{t}_1 < \tilde{t} < \tilde{t}_2$, and maintains a velocity of zero for $\tilde{t} > \tilde{t}_2$. The values of \tilde{t}_0 , \tilde{t}_1 , \tilde{t}_2 and \tilde{U}_p for each of the four cases considered are given in table 1. The term \tilde{U}_p is used as the velocity scale in this case. This table also includes the experimentally observed time \tilde{t}_p at which the instability sets in and the values of the Reynolds number based on \tilde{U}_p and the radius of the pipe. In this case, Das & Arakeri (1998) found an analytical solution for the velocity distribution in terms of an infinite series containing Bessel functions. The velocity profiles for the four cases reported in table 1 are plotted in figure 2.

Finally, the base flow profiles for laminar flows in a reservoir–pipe–valve system, where the transient is triggered by an instantaneous closure of the valve, are derived by Hall & Parker (1976) using a type of Pohlhausen technique and by Ghidaoui & Kolyshkin (2001, 2002) using the method of Laplace transform. If the flow before the sudden blockage was steady pipe Poiseuille flow, then the solution obtained by Ghidaoui & Kolyshkin (2002) has the form

$$W(r, \hat{t}) = \sum_{n=1}^{\infty} \frac{2J_1(\beta_n) - \beta_n J_0(\beta_n r)}{\beta_n^2 J_1(\beta_n)} \exp(-\beta_n^2 \hat{t}), \tag{3}$$

where $\hat{t} = t/Re$; $J_m(q)$ is a Bessel function of the first kind of order m ; and β_n are the roots of the equation $J_2(\beta_n) = 0$. Here and in the rest of the paper the variables without tildes are dimensionless variables such that the measures of length, time, pressure and velocity are R , R/\tilde{U}_c , $\rho\tilde{U}_c^2$ and \tilde{U}_c , respectively, where \tilde{U}_c is the velocity at the axis of the pipe for steady state and R is the radius of the pipe; the Reynolds number is defined by the formula $Re = R\tilde{U}_c/\nu$. To avoid confusion, Re_D is used to denote the Reynolds number based on mean velocity and pipe diameter.

The linear stability of three types of base flow discussed above is studied in this paper. The results of numerical simulation are compared with the experimental data of Lefebvre & White (1989) and Das & Arakeri (1998).

2.2. Stability, perturbation equations and solution procedure

We seek to study the stability of the unsteady one-dimensional non-periodic base flows discussed in the previous section. Recall that the base flow $W(r, t)$ and $P(z, t)$ represent the dimensionless solution of (2) subject to appropriate boundary conditions such as valve closure or valve opening and to initial condition $W(r, 0)$

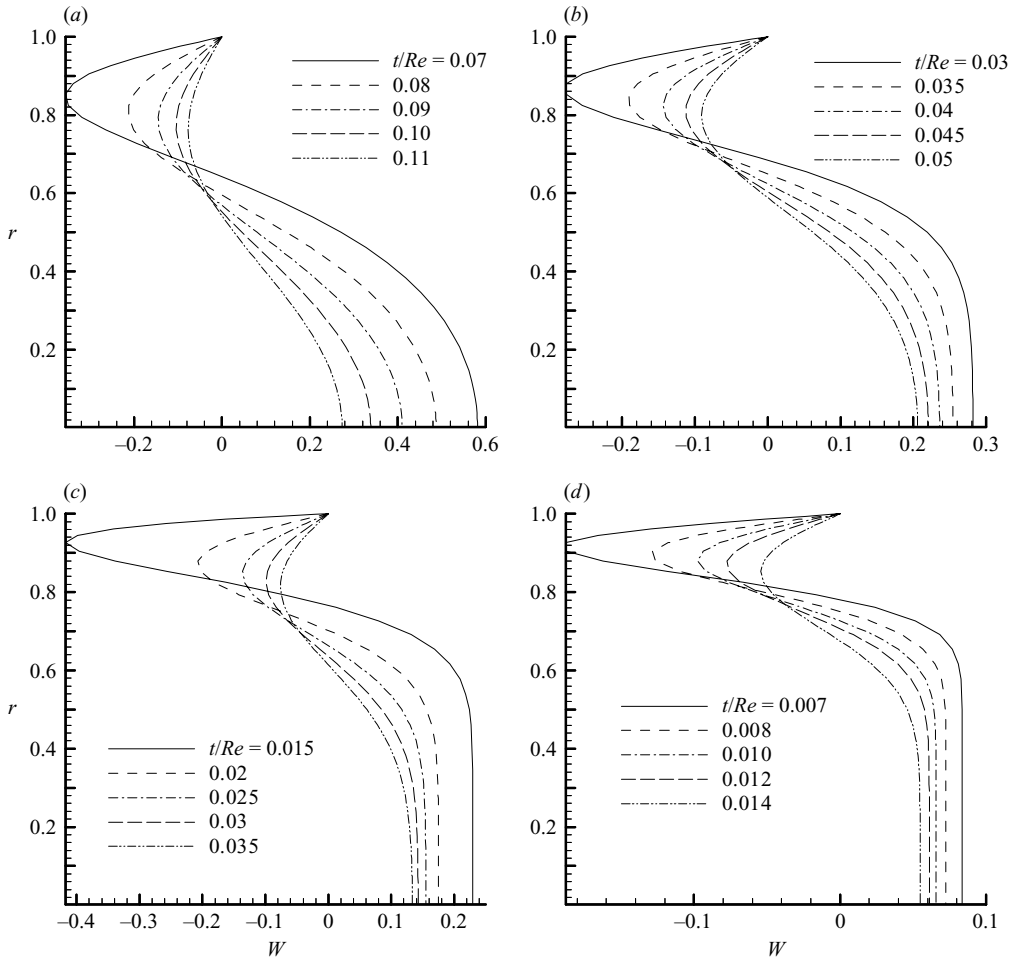


FIGURE 2. Base flow profiles for decelerated flows (Das & Arakeri 1998). (a) Case I, (b) Case II, (c) Case III, (d) Case IV.

and $P(z, 0)$. Let $W(r, t)\mathbf{k} + \mathbf{u}(\mathbf{x}, t)$ and $P(r, t) + p(\mathbf{x}, t)$ denote the solution of the Navier–Stokes equations subject to the perturbed initial condition $W(r, 0)\mathbf{k} + \mathbf{u}(\mathbf{x}, 0)$ and $P(r, 0) + p(\mathbf{x}, 0)$, where $\mathbf{x} = (r, \theta, z)$, θ is the azimuthal coordinate, z is the longitudinal (streamwise) coordinate, \mathbf{k} is the unit vector in the longitudinal direction, $\mathbf{u}(\mathbf{x}, t) = (u(r, \theta, z, t), v(r, \theta, z, t), w(r, \theta, z, t))$ is the velocity field of the perturbation, and $\mathbf{u}(\mathbf{x}, 0) = (u(r, \theta, z, 0), v(r, \theta, z, 0), w(r, \theta, z, 0))$ is the initial (imposed) velocity perturbation. Note that $\mathbf{u}(\mathbf{x}, t)$, being the difference between the base field and the perturbed field, describes how far the perturbed field is from the base flow. Stability is achieved if $\mathbf{u}(\mathbf{x}, t)$ is found to die away with time so that the perturbed field eventually returns to the base field. A measure of how far has the perturbed velocity field departed from the base flow field at time t over volume $[0, 1] \times [0, 2\pi] \times [0, 2\pi/\alpha]$ is given by the following norm of $\mathbf{u}(\mathbf{x}, t)$:

$$\langle |\mathbf{u}|^2 \rangle = \frac{1}{V} \int_0^{2\pi/\alpha} \int_0^{2\pi} \int_0^1 \mathbf{u} \cdot \mathbf{u} r \, dr \, d\theta \, dz = \frac{1}{V} \int_0^{2\pi/\alpha} \int_0^{2\pi} \int_0^1 (u^2 + v^2 + w^2) r \, dr \, d\theta \, dz \tag{4}$$

where $\mathcal{V} = 4\pi^2/\alpha$. The norm given by (4) is twice the average kinetic energy, $E(t)$, over volume $[0, 1] \times [0, 2\pi] \times [0, 2\pi/\alpha]$ (i.e. $E(t) = \langle |\mathbf{u}|^2 \rangle / 2$). Note that this volume defines a pipe section whose streamwise length is equal to one full wave length $2\pi/\alpha$.

The evolution of the volume-averaged kinetic energy of perturbation (disturbance) is given by (e.g. Joseph 1976; Schmid & Henningson 2001)

$$\frac{dE}{dt} = \frac{1}{\mathcal{V}} \int_0^{2\pi/\alpha} \int_0^{2\pi} \int_0^1 uv \frac{dW}{dr} r dr d\theta dz - \frac{1}{Re\mathcal{V}} \int_0^{2\pi/\alpha} \int_0^{2\pi} \int_0^1 \nabla \mathbf{u} \cdot \mathbf{u} r dr d\theta dz \quad (5)$$

where ∇ is the gradient operator in cylindrical polar coordinates. Clearly, the norm of difference between the base field and the perturbed field, measured by a volume-averaged kinetic energy, depends on Reynolds number, the exchange of energy between the base flow and the perturbations and the dissipation of perturbations by viscous effects.

The behaviour of $E(t)$, which is a measure of the deviation of the perturbed field from the base field, is central to the investigation of the stability of the base flow $W(r, t)$ and $P(z, t)$. Evaluation of the right-hand side of (5) requires the solution of the equations which give the perturbation field $\mathbf{u}(\mathbf{x}, t) = (u(r, \theta, z, t), v(r, \theta, z, t), w(r, \theta, z, t))$ subject to boundary conditions and initial conditions $\mathbf{u}(\mathbf{x}, 0) = (u(r, \theta, z, 0), v(r, \theta, z, 0), w(r, \theta, z, 0))$. To this end, using the Navier–Stokes equations and considering that the infinitesimal perturbations are

$$\begin{aligned} & [u(r, \theta, z, t); v(r, \theta, z, t); w(r, \theta, z, t); p(r, \theta, z, t)]^T \\ & = [\hat{u}(r, t); \hat{v}(r, t); \hat{w}(r, t); \hat{p}(r, t)]^T \exp(in\theta + i\alpha z) \quad (6) \end{aligned}$$

where α is the axial wavenumber; n is the azimuthal wavenumber; and $\hat{u}, \hat{v}, \hat{w}, \hat{p}$ are the amplitudes of perturbation corresponding to u, v, w, p , respectively, we obtain

$$\frac{1}{r} \frac{\partial(r\hat{u})}{\partial r} + \frac{in}{r} \hat{v} + i\alpha \hat{w} = 0 \quad (7)$$

$$\frac{\partial \hat{u}}{\partial t} + i\alpha W \hat{u} = -\frac{\partial \hat{p}}{\partial r} + \frac{1}{Re} \left(N \hat{u} - \frac{\hat{u}}{r^2} - \frac{2in}{r^2} \hat{v} \right) \quad (8)$$

$$\frac{\partial \hat{v}}{\partial t} + i\alpha W \hat{v} = -\frac{in}{r} \hat{p} + \frac{1}{Re} \left(N \hat{v} - \frac{\hat{v}}{r^2} + \frac{2in}{r^2} \hat{u} \right) \quad (9)$$

$$\frac{\partial \hat{w}}{\partial t} + i\alpha W \hat{w} + \hat{u} \frac{\partial W}{\partial r} = -i\alpha \hat{p} + \frac{1}{Re} N \hat{w} \quad (10)$$

where

$$N = \frac{\partial^2}{\partial r^2} + \frac{1}{r} \frac{\partial}{\partial r} - \frac{n^2}{r^2} - \alpha^2.$$

The boundary conditions at the wall $r = 1$ are

$$\hat{u}(1, t) = 0, \quad \hat{v}(1, t) = 0, \quad \hat{w}(1, t) = 0, \quad \left. \frac{\partial \hat{u}(r, t)}{\partial r} \right|_{r=1} = 0. \quad (11)$$

The boundary conditions at the pipe centreline depend on the azimuthal wavenumber and have the form (for details see Moin & Kim 1980; Lopez, Marques & Shen 2002).

For $n = 0$,

$$\hat{u}(0, t) = 0, \quad \hat{v}(0, t) = 0, \quad \hat{w}(0, t) \equiv \text{finite}, \quad \hat{p}(0, t) \equiv \text{finite}. \quad (12)$$

For $n = 1$,

$$\hat{u}(0, t) + i\hat{v}(0, t) = 0, \quad \hat{w}(0, t) = 0, \quad \hat{p}(0, t) = 0, \quad \left[\frac{\partial \hat{u}(r, t)}{\partial r} + i \frac{d\hat{v}(r, t)}{dr} \right] \Big|_{r=0} = 0. \quad (13)$$

For $n = 2, 3, \dots$,

$$\hat{u}(0, t) = 0, \quad \hat{v}(0, t) = 0, \quad \hat{w}(0, t) = 0, \quad \hat{p}(0, t) = 0. \quad (14)$$

The behaviour of the velocity field of perturbations $\mathbf{u}(\mathbf{x}, t) = (u(r, \theta, z, t), v(r, \theta, z, t), w(r, \theta, z, t))$, as well as the kinetic energy of perturbations depend on the perturbation imposed at $t = 0$, namely, $\mathbf{u}(\mathbf{x}, 0) = (u(r, \theta, z, 0), v(r, \theta, z, 0), w(r, \theta, z, 0))$. The role of initial conditions on the perturbation dynamics of small disturbances in a plane Poiseuille flow is discussed in Criminale *et al.* (1997). They used different initial conditions (symmetric, antisymmetric, localized or more spread across the channel) in order to analyse the growth of perturbation energy for different times. One of the objectives of their paper was to determine whether the large optimal transient growth obtained in the previous studies could be realized by arbitrary initial conditions. The calculations presented in Criminale *et al.* (1997) show that the calculated transient growth for arbitrary initial conditions for two-dimensional disturbances in plane Poiseuille flow is found to be about 25 % of the optimal.

Two approaches are used in the present paper to analyse the behaviour of small perturbations in unsteady pipe flows. First, arbitrary disturbances in an unforced media are simulated by means of uncorrelated random initial conditions. The calculations are done for different initial conditions. In addition, the sample average is analysed as well. The use of different random initial conditions will also help to answer the question of whether the transient growth is associated with only certain initial conditions. Secondly, optimal perturbations are also considered in order to obtain maximum transient growth amplification. Following the conclusions from Criminale *et al.* (1997), it is plausible to assume that, most probably, the large optimal transient growth does not take place in practice unless a carefully controlled perturbation generator is used. However, the optimal energy growth curve is usually considered as a reference point and serves as the basis for discussion related to the bypass transition scenario. If the optimal energy growth is large enough, then there is a possibility of the bypass transition.

Optimal initial perturbations have been extensively studied by Butler & Farrell (1992) for plane channel flow and Bergström (1993) and Schmid & Henningson (1994) for pipe Poiseuille flow. In these studies, the initial condition that can achieve maximum amplification of initial energy is searched for. The maximum transient growth at $\alpha = 0$ and $n = 1$ produced by optimal initial perturbation is about $E(t)/E(0) = 7 \times 10^{-5} Re^2$, at time $t = 0.048 Re$, as obtained by Schmid & Henningson (1994) for the case of pipe Poiseuille flow, which is essentially the same as that produced by the initial condition of Bergström (1992).

The growth of a perturbation at a particular time t_p can be described by the function $G(t_p) = E(t_p)/E(0)$ if the base flow and initial perturbations $\hat{u}(r, 0)$, $\hat{v}(r, 0)$ and $\hat{w}(r, 0)$ are specified. Variational techniques are used by Butler & Farrell (1992) and Bergström (1993) to investigate the optimal growth for plane Poiseuille, Couette, Blasius and pipe Poiseuille flows. For example, Bergström (1993), in a study of a pipe Poiseuille flow, represented an arbitrary disturbance as a sum of damped modes of the system and then used the variational principle to calculate the largest possible amplification of the energy at time t_p .

In the present study, it is not proper to express the perturbation in terms of eigenmodes since the base flow is unsteady. The approach which is based on a nonlinear optimization is employed below. For a given set of initial values $\hat{u}(r, 0)$, $\hat{v}(r, 0)$ and $\hat{w}(r, 0)$ we calculate $G(t_p)$ using the initial-value problem solver. Thus, $G(t_p)$ is a nonlinear function of $\hat{u}(r, 0)$, $\hat{v}(r, 0)$ and $\hat{w}(r, 0)$. Our goal is to find $\hat{u}(r, 0)$, $\hat{v}(r, 0)$ and $\hat{w}(r, 0)$ in order to maximize $G(t_p)$ at time t_p . This is a typical nonlinear optimization problem which we solve by means of DOT (design optimization tools) software developed by Vanderplaats Research & Development. A finite-difference approach is used by DOT in order to provide the gradients required to change the decision variables and optimize the object function G . The use of finite differences is particularly useful since the derivatives of the object function with respect to the decision variables cannot be calculated analytically. Three types of search strategy are used, namely, a modified feasible directions algorithm, a sequential linear programming method and a sequential quadratic programming method. It is found that all three methods converge to the same optimal initial conditions, the only difference is the rate of convergence. All the results generated in the paper are obtained by means of a modified feasible directions algorithm and a sequential linear programming method.

System (7)–(10) is solved using a semi-implicit scheme (Moin & Kim 1980). The convective terms are approximated by the second-order Adams–Bashforth scheme while the second-order Crank–Nicolson scheme is used for viscous and pressure terms. Chebyshev polynomials are used for discretization in the radial direction. Details of the numerical scheme are described in Zhao, Ghidaoui & Kolyshkin (2004). The study of the complete perturbation dynamics and the analysis of both short-time and long-time transients can now be investigated as an initial-boundary value problem, where (7)–(10) is solved subject to boundary conditions (11)–(14) and to different initial conditions ranging from random to optimal. Using this approach, we can trace the evolution of any small perturbation in the flow. The procedure of solving the perturbation equations by numerical integration is hereinafter referred to as linearized direct numerical simulation (L-DNS).

3. Results and discussion

We begin by validating the linear model against published results such as those in Schmid & Henningson (1994). Schmid & Henningson (1994) calculated the transient growth for pipe Poiseuille flow and provide detailed results for $Re=1000$ and wavenumbers $\alpha=0, n=1$. It should also be noted that $\alpha=0$ and $n=1$ are known to produce the maximum temporal growth of perturbations in pipe flow (Ben-Dov, Levinski & Cohen 2003; Schmid & Henningson 1994). The current model is applied to the same conditions as those in Schmid & Henningson (1994), and the results are presented in figure 3. The energy evolution curves are plotted for different random initial conditions together with the averaged result (solid line). The dotted lines represent each of the 25 samples used in the simulation. In addition, the optimal growth curve (dashed line) is also shown for comparison. The behaviour of the growth curves is similar to the behaviour of the optimal perturbations except that the maximum growth for the averaged result based on random initial conditions ($E(t)/E(0) = 1.65 \times 10^{-5} Re^2$) is about a quarter of the optimal growth. The maximum amplification factor is 71.9 which is close to the value of 72 calculated by Schmid & Henningson (1994). The maximum growth occurs at time $t = 0.049Re$ (the maximum growth for the averaged result occurs a little earlier at time $t = 0.048Re$). The

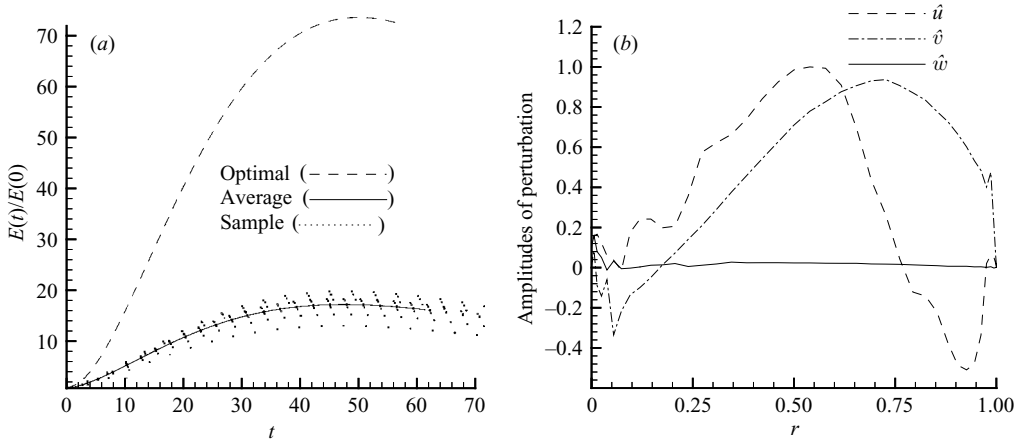


FIGURE 3. (a) Transient growth of random initial conditions and optimal initial condition for Poiseuille flow ($Re = 1000$, $\alpha = 0$, $n = 1$). (b) Optimal initial perturbations $\hat{u}(r, 0)$, $\hat{v}(r, 0)$ and $\hat{w}(r, 0)$ versus r which produces maximum G at $t = 49$.

simulation results in figure 3 show that transient growth is not associated with a particular type of initial perturbation. In addition, figure 3(b) shows that the axial component of the optimal initial perturbation is almost zero in agreement with the results obtained by Schmid & Henningson (1994).

The dependence of the norm of perturbations on initial conditions $\hat{u}(r, t = 0)$, $\hat{v}(r, t = 0)$, $\hat{w}(r, t = 0)$ is analysed as follows. A random number from a standardized normal distribution is generated for $\hat{u}(r, t = 0)$, $\hat{v}(r, t = 0)$, $\hat{w}(r, t = 0)$ at each radial node. Only those initial conditions that are divergence free are considered as initial conditions for the linear initial boundary-value problem. The divergence-free initial condition is obtained as follows. A random velocity field is generated. Since it is unlikely that this random field is divergence free, a process to render it divergence free (i.e. to ensure that the initial field satisfies mass balance) is required. The inviscid form of (7)–(10) and the non-divergent randomly generated velocity field are solved. During this solution, the pressure terms redistribute the random velocity field and if the model is run for a long enough time, the flow redistribution will ensure that the flow field satisfies mass (i.e. divergence-free velocity field) and momentum. The resulting divergence-free field constitutes the initial perturbation which when solved together with (7)–(10) and (11)–(14) provides a complete solution for how the perturbations behave with time.

Different values of n and α are used for the analysis of water hammer flow. Linear stability calculations with a quasi-steady assumption by Ghidaoui & Kolyshkin (2001) show that (i) the least stable mode for all times tested is the mode with $n = 1$, and (ii) that the critical wavenumbers vary from $\alpha = 1.2$ to $\alpha = 1.6$ in the interval $0.001 \leq \hat{t} \leq 0.02$, which contains the ‘least stable’ velocity profile. Taking this information into account, the results are presented for $n = 1$ and $\alpha = 1.5$. Figure 4(a) is plot of energy growth curves of a perturbation for the least stable modes. The instantaneous slopes of the curves are the growth rates of perturbation energy for the instantaneous velocity profile, that is,

$$G_E(t) = \lim_{\Delta t \rightarrow 0} \frac{\ln E(t + \Delta t) - \ln E(t)}{\Delta t} \quad (15)$$

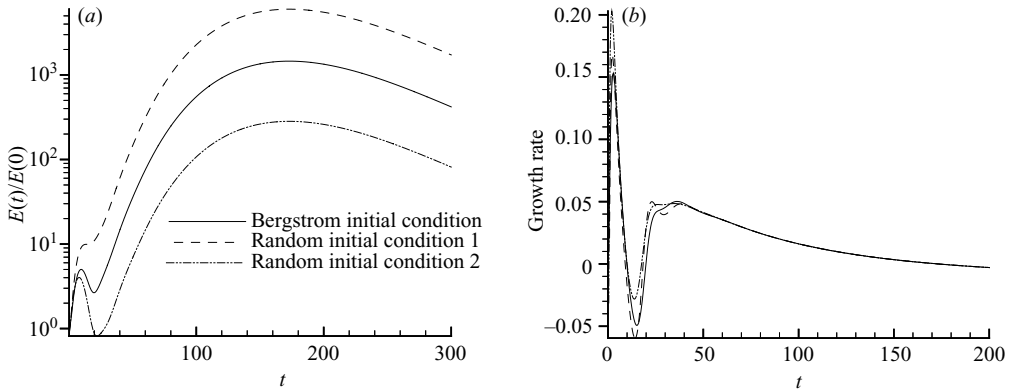


FIGURE 4. Growth behaviour of perturbations for water hammer flow ($Re = 2000, \alpha = 1.5, n = 1$), (a) growth and (b) growth rate for different initial conditions.

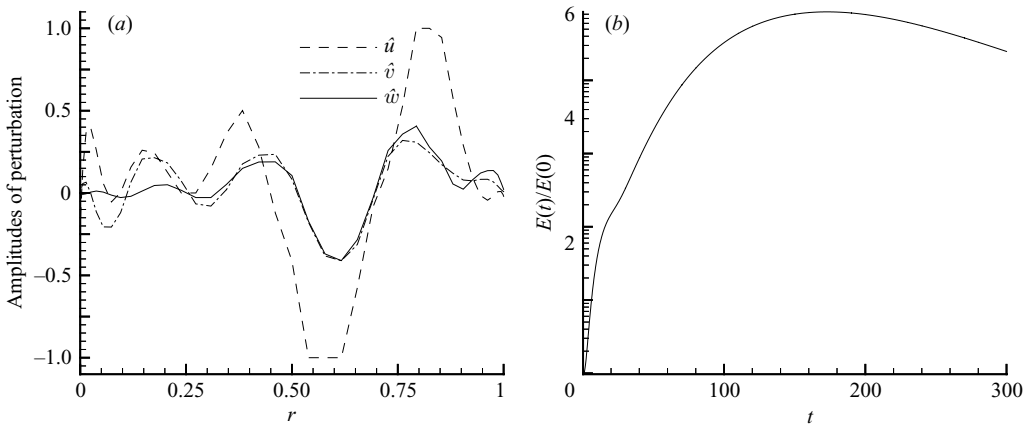


FIGURE 5. (a) Amplitudes of optimal initial perturbations as a function of r which maximize G at $t = 300$ and (b) transient growth for the optimal perturbation for water hammer flow ($Re = 2000, \alpha = 1.5, n = 1$).

It can be seen from the figure that energy growth curves behave differently for small times ($t < 40$), but for $t > 40$, the growth curves are essentially parallel to each other (that is, the slopes of the tangent lines to all three curves are almost the same for large times). This is also shown in figure 4(b). For $t < 40$, the growth rates for different initial conditions are not the same, but for $t > 40$, the dependence of the growth rates on the initial condition disappears and different initial conditions give the same growth rates.

Although the growth rates for large times are independent of initial condition, the total energy at time t depends on the initial condition since it is proportional to the integral of the growth rates evaluated from $t = 0$ to time t . Figure 4(a) also shows that the maximum perturbation energy with one initial condition can differ from that with another initial condition by a factor of 10 or 20.

Optimal initial conditions for waterhammer flow with $Re = 2000$ and $\alpha = 1.5$ together with the optimal energy growth curve are shown in figure 5. It is seen from figure 5 that qualitative behaviour of the optimal growth curve for large times is similar to the behaviour of the growth curves for different initial conditions (see

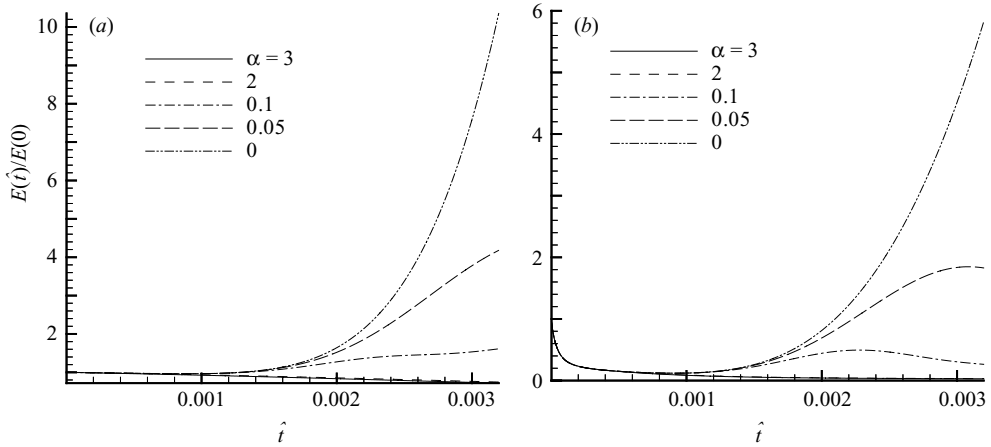


FIGURE 6. Energy growth for different initial conditions for (Das & Arakeri 1998; Case 1 where the Reynolds number based on mean velocity and diameter is $Re_D = 2.4 \times 10^5$ and the measured transitional time is $\hat{t} = 0.0032$). (a) Bergström initial condition and (b) random initial condition.

figure 4). However, depending on the initial condition, the magnitude of energy growth can differ by a factor of 100 from the optimal case.

3.1. Flow stability of accelerated flows

Henningson & Reddy (1994) and Schmid & Henningson (2001) show that the kinetic energy of infinitesimal perturbations (linear analysis) and of finite-amplitude perturbations (nonlinear analysis) obey the same relation, namely, equation (5). This is because the nonlinear terms are conservative and their role is to redistribute the energy between different spatial scales. As a result, they argued that the growth rate of a large-amplitude perturbation at instant t is equal to that of an infinitesimal perturbation whose shape is identical to the large-amplitude perturbation and showed that linear mechanisms in the form of exponential, algebraic or transient growth are necessary conditions for flow transition. The more substantial is the transient energy growth of a given flow, the more likely that this flow exhibits transition to a turbulent state or to a different, often more complex, laminar state. The transient growth and its role in the stability of accelerating as well as decelerating flows in pipes are studied in the remainder of this paper.

Stability of laminar flows in a pipe subject to a rapid acceleration is studied experimentally by Lefebvre & White (1989). In their study, a control valve is used to create a constant acceleration from rest to a certain mean velocity. The measured shear stress traces show bursts indicating transition during the acceleration. Experimental transition times and transition Reynolds numbers are obtained in their experiments.

We study the evolution of a perturbation by solving the corresponding initial-value problem. The energy growth of perturbations with different axial wavenumbers is shown in figure 6(a) when the Bergström (1992) initial condition is used. The parameters of the flow correspond to the experimental data of Lefebvre & White (1989). In particular, two cases are investigated in this paper. Case 1 correspond to a diameter-based Reynolds number of 2.4×10^5 . The measured transition time \hat{t} for Case 1 is about 0.0032. Case 2 correspond to a diameter-based Reynolds number of 5.2×10^5 . The measured transition time t for Case 2 is about 0.00105.

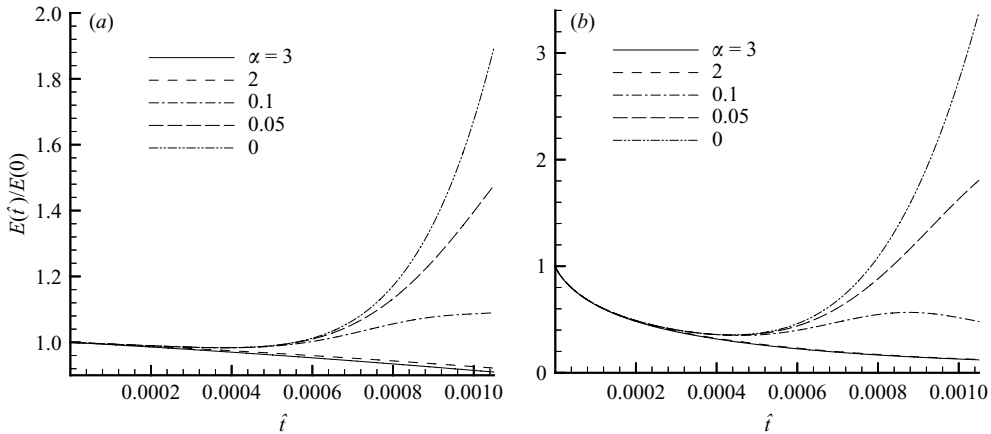


FIGURE 7. Perturbation growth for accelerated flow (Lefebvre & White 1989; Case 2 where the Reynolds number based on mean velocity and diameter is $Re_D = 5.2 \times 10^5$ and the measured transitional time is $\hat{t} = 0.00105$). (a) Bergström initial condition and (b) random initial condition.

The computations were carried out for a variety of wavenumber α and n . We found that $n = 1$ and $\alpha = 0$ are the most unstable in the sense that, for given initial and boundary conditions, the largest transient growth was obtained when $n = 1$ and $\alpha = 0$. It is seen from figure 6(a) that perturbations with small axial wavenumbers α grow quickly starting from $t = 0.001$. In fact, the energy growth beyond $t = 0.001$ becomes more pronounced for perturbations with longer wavelength along the streamwise direction (i.e. waves with small α). The linear growth of \hat{w} is induced by the tilting of vorticity by the radial component of the velocity perturbation. The transition to turbulence was observed experimentally at $t = 0.0032$. Figure 6(a) shows that the energy of the least stable mode ($n = 1$ and $\alpha = 0$) increases tenfold at $t = 0.0032$. In addition, the energy of perturbations that is weakly dependent on the streamwise direction (e.g. energy curve for $\alpha = 0.05$) also experiences significant growth between $\hat{t} = 0.001$ and $\hat{t} = 0.0032$. It is plausible to assume that the transient growth is responsible for the transition to turbulence in this case.

Similar calculations are performed for different randomly distributed initial conditions. It is found that for some sets of random initial conditions there is no perturbation growth whereas other random initial conditions show growth behaviour qualitatively similar to the Bergström initial condition. One case of a random initial condition which leads to energy growth of the perturbation is illustrated in figure 6(b). Comparing the graphs in figures 6(a) and 6(b), we can see qualitatively similar behaviour of growth curves after $t = 0.001$. Despite the fact that the perturbation with random initial condition and small axial wavenumber initially decays, it starts to grow after $t = 0.001$ in a similar way to the case with the Bergström initial condition. At $t = 0.0032$, the perturbation associated with the most unstable mode grows sixfold.

Figure 7 shows the growth of perturbations for another case (Lefebvre & White 1989; Case 2); similar behaviour to the previous case is revealed. The Reynolds number based on the final mean velocity and diameter is 5.2×10^5 , and the measured transition time t is about 0.00105.

The amplitudes of optimal initial perturbations and the corresponding growth curves for optimal perturbations are shown in figures 8 and 9 for experimental Cases 1 and 2 in Lefebvre & White (1989), respectively, where the optimization is

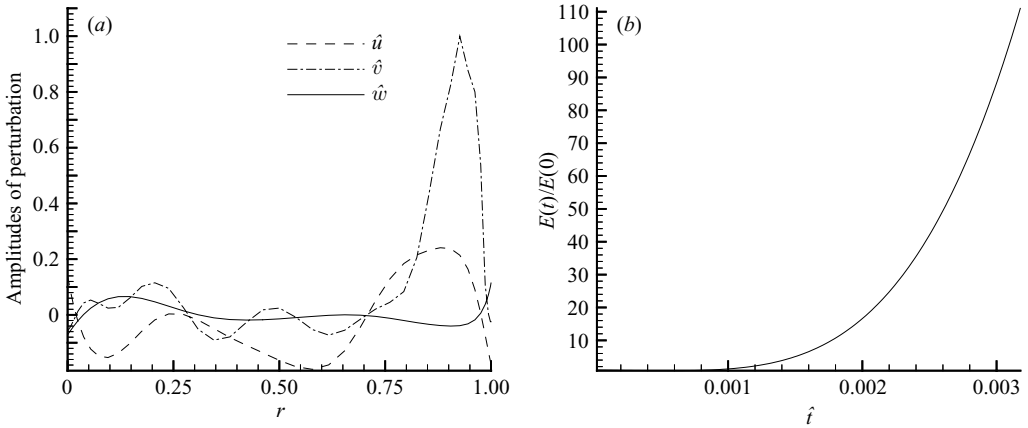


FIGURE 8. (a) Amplitudes of optimal initial perturbation as a function of r which maximize G at $\hat{t} = 0.0032$. (b) Transient growth for the optimal perturbation for accelerated flow (Lefebvre & White 1989; Case 1, $Re_D = 2.4 \times 10^5$) ($\alpha = 0$).

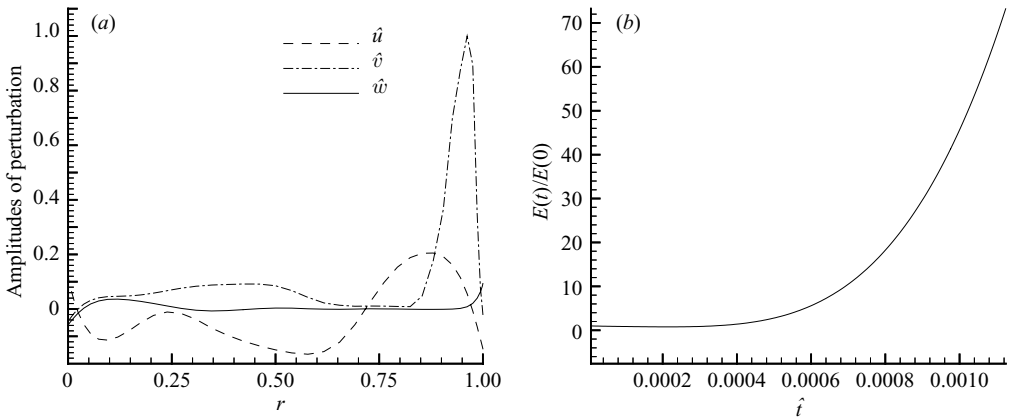


FIGURE 9. (a) Amplitudes of optimal initial perturbation as a function of r which maximize G at $\hat{t} = 0.0013$. (b) Transient growth for the optimal perturbation for accelerated flow (Lefebvre & White 1989; Case 2, $Re_D = 5.2 \times 10^5$) ($\alpha = 0$).

performed at time $t = 0.0032$ for Case 1 and $t = 0.0013$ for Case 2. In both cases, the corresponding wavenumber of the perturbation is that of the most unstable mode. Comparing figures 6 and 7 for different initial conditions with the corresponding graphs in figures 8 and 9, we can see that, as in the case of accelerated flow, the qualitative behaviour of the growth curves for arbitrary initial perturbations and optimal initial perturbations is similar. The only important difference is the magnitude of the growth.

The above results show that the largest growth rate occurs when the perturbations are independent of the streamwise coordinate (i.e. $\alpha = 0$). Ellingsen & Palm (1975) investigated the behaviour of perturbations that are independent of the streamwise coordinate (i.e. $\alpha = 0$). They found that the streamwise perturbations and the kinetic energy of these perturbations grows linearly with time, even when the base flow does not contain inflection points. A similar derivation can be performed here. In particular, considering perturbations that are independent of the streamwise coordinate (i.e. $\alpha = 0$) and since this is a high-Reynolds-number flow reduces (8) and

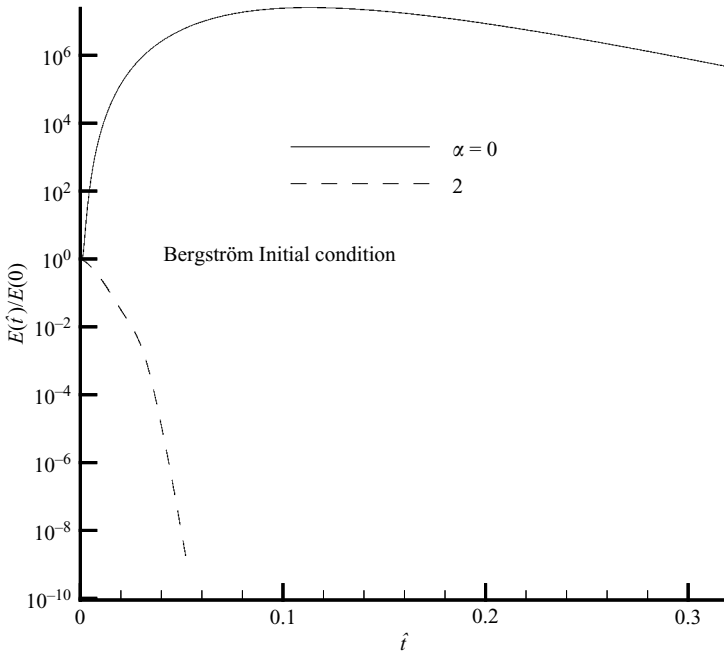


FIGURE 10. Long-time behaviour of growth of perturbation.

(10) to $\hat{u} \approx \text{constant}$ with respect to time and $\hat{w} = w_0 - t\hat{u}(\partial W/\partial r)$. Indeed, figures 6 and 7 show that the energy grows the most when $\alpha = 0$ and that this growth becomes linear in time for large t . The instability associated with small values of α manifests itself in the form of streaks oriented in the streamwise direction (Butler & Farrel 1992).

The long-term behaviour of energy growth of perturbations for Case 1 in Lefebvre & White (1989) is shown for $\alpha = 0$ and $\alpha = 2$ in figure 10. It is seen from the figure that, for large times, the perturbations in the flow accelerated from rest asymptotically decay. A quasi-steady assumption is also used in order to study linear stability of flow accelerated from rest. Linear stability calculations are performed for different values of the Reynolds number. Numerical results indicate that the flow is linearly stable (the detailed results are not shown here) in the range of Reynolds numbers reported by Lefebvre & White (1989).

The method of normal modes together with the quasi-steady assumption (which assumes that the mean velocity profiles are ‘frozen’) is often used in stability studies of unsteady non-periodic viscous flows. Perturbation energy decay for large times corresponds to linear stability of the base flow since the growth rate is negative in this case. This means, in particular, that the transition in the case of pipe flows accelerated from rest cannot be explained by the exponential growth of a mode.

3.2. Flow stability of decelerated flows

Decelerated flows studied by Das & Arakeri (1998) have different features from the accelerated flows studied by Lefebvre & White (1989). The obvious difference between the base flows in figure 1 and that in figure 2 is the presence of inflection points in the velocity profiles in figure 2.

Das & Arakeri (1998) used a dye-visualization method to observe how the flow becomes unstable. For this purpose, the time \tilde{t}_p when the dye line takes the form of a wave (in other words, the time when a perceptible wave appears) is measured. Energy

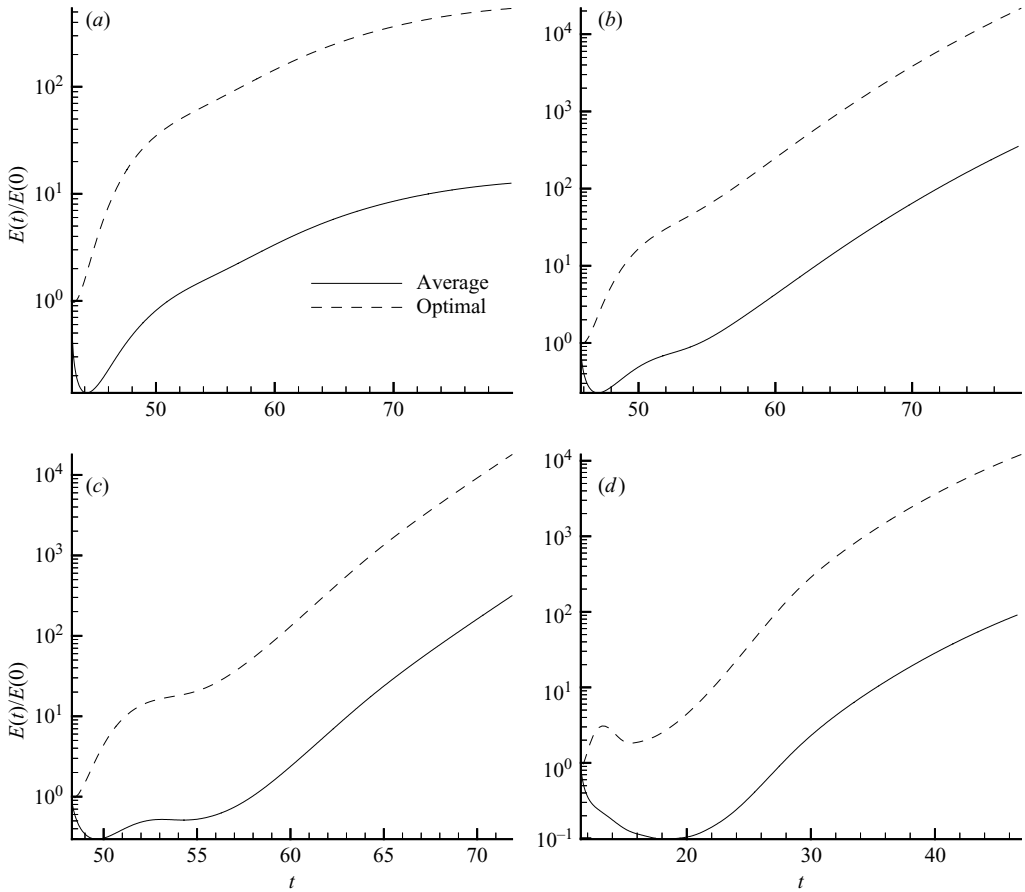


FIGURE 11. Growth of perturbations for decelerated flows (Das & Arakeri 1998). (a) Case I ($\alpha = 1.77, n = 1$), (b) Case II ($\alpha = 2.65, n = 1$), (c) Case III ($\alpha = 3.37, n = 1$), (d) Case IV ($\alpha = 5.50, n = 1$).

growth curves of perturbations in decelerated flows (Cases I–IV for the experiments of Das & Arakeri 1998) are plotted in figure 11. The solid curves in figure 11 represent the sample average (25 random initial conditions are used). The corresponding graphs for optimal perturbations are also shown in these figures. As can be seen from the graphs, all four solid curves exhibit a similar behaviour: initial energy decay is followed by energy growth at larger times. A possible reason for the decay is that the initial condition includes many modes, most of them decay with time. The energy begins to grow after a certain time since at that time the perturbation contains a few unstable modes. Note that the perturbation growth for each case is associated with critical wavenumber and is calculated until the perturbation is found to be perceptible in the experiments. The critical wavenumber is the wavenumber at which, for a particular initial condition, the maximum growth is obtained at the perceptible time. The same approach is used by Chen & Kirchner (1971) to determine the fastest-growing wave. Note that different initial conditions might give different critical wavenumbers so that the results obtained from different random initial conditions are averaged. In all the examples, fewer than 40 samples are used for each case. The non-dimensional critical wavenumbers are given in the last column of table 2.

Case	$(\lambda/\delta_*)_{exp}$	$(\lambda_{max}/\delta_*)_{DA}$	$(\lambda_{max}/\delta_*)_{GK}$	(λ_{max}/δ_*)	α
I	3.2	4.0	3.7	3.8	1.77
II	2.7	4.2	2.8	3.0	2.65
III	3.1	5.0	2.7	3.3	3.37
IV	3.0	3.3	2.6	2.5	5.50

TABLE 2. Scaled wavelengths and critical wavenumbers, where experimental data are represented by the subscript ‘*exp*’, the results of Das & Arakeri (1998) are represented by the subscript ‘*DA*’, the calculations by Ghidaoui & Kolyshkin (2002) are represented by the subscript ‘*GK*’, λ = wavelength; δ_* = average boundary-layer thickness taken over the time \tilde{t}_1 to \tilde{t}_p ; subscript ‘*max*’ means that the wavelength corresponds to maximum growth rate in ‘*DA*’ and ‘*GK*’ and the maximum energy growth in the present model.

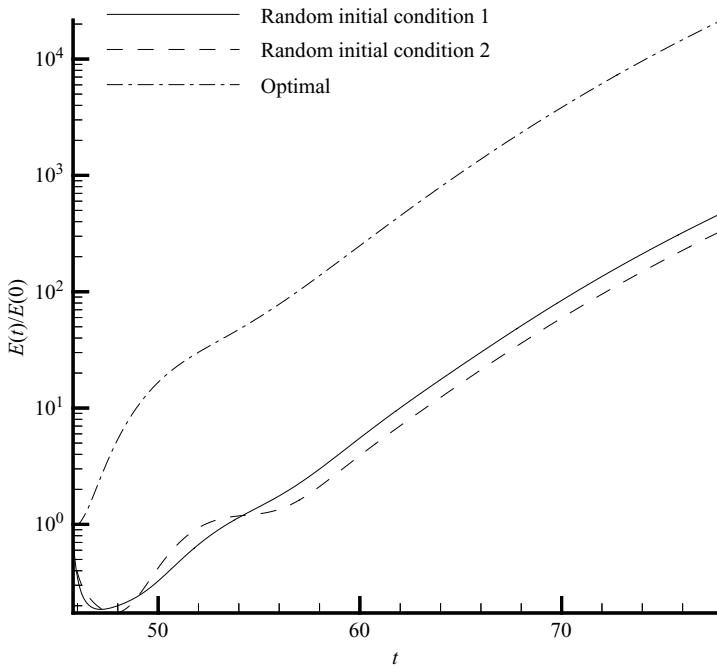


FIGURE 12. Energy growth for different initial conditions for Case II ($\alpha = 2.65, n = 1$).

Figure 12 shows energy growth curves for optimal perturbations and two different random initial conditions (referred to as ‘initial condition 1’ and ‘initial condition 2’ in the remaining part of the paper). The energy growth evolution is calculated for $\alpha = 2.65$ and $n = 1$. It is seen from the graph that before $t = 60$, the energy growth depends on the initial condition. However, after $t = 60$, all three curves are parallel to each other in the semi-log plot, which means that the same growth rates are achieved. To shed light on this behaviour of the perturbations, the flow structure at $t = 50$ and $t = 78$ is investigated. It is seen from the contour plots of radial vorticity ($\zeta_r = (1/r)(\partial w/\partial \theta) - (\partial v/\partial z)$) in figure 13 at $t = 50$ that the contour patterns for different random initial conditions are totally different. This is because, for random initial condition 2 at $t = 50$, the perturbation is not yet organized whereas for random initial condition 1, the pattern appears to be more or less regular. At $t = 78$, the contour plots for different random initial conditions are very similar, the only difference being

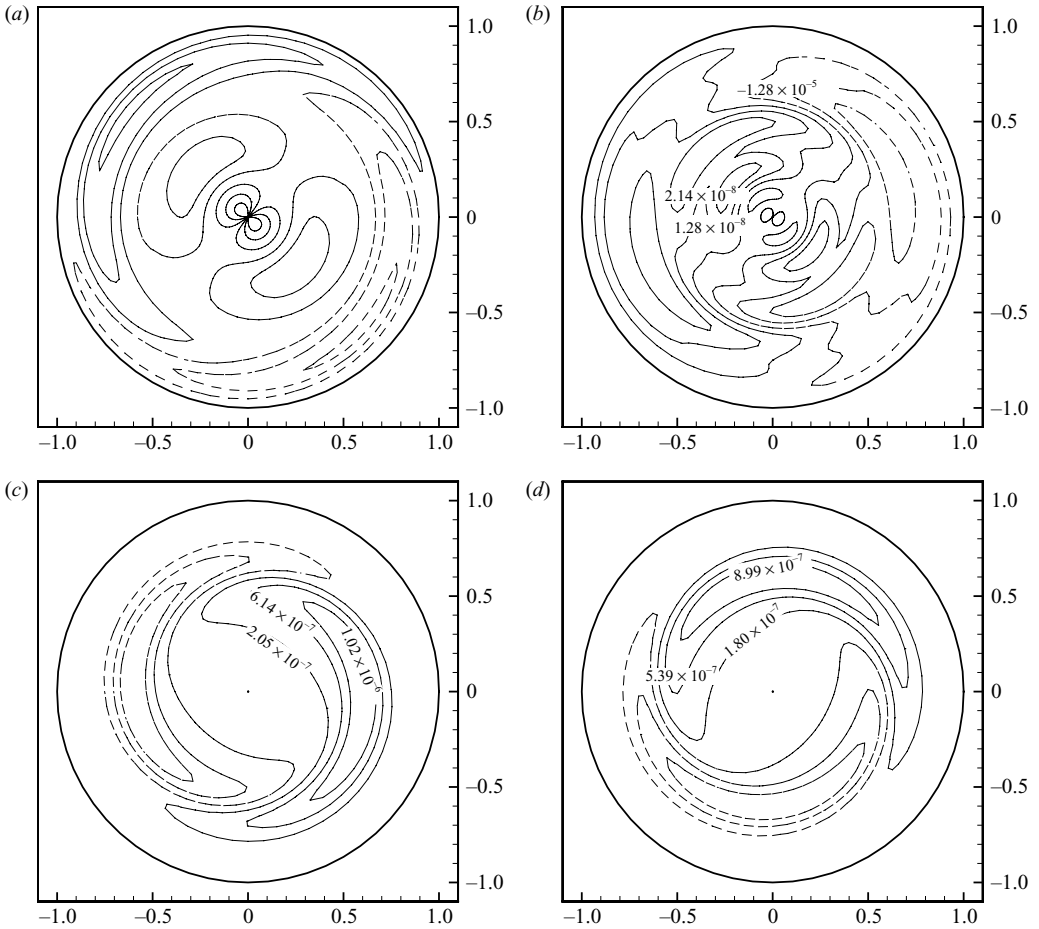


FIGURE 13. Vorticity contours at different times for different initial conditions for Case II ($\alpha = 2.65$, $n = 1$). (a) $t = 50$, random initial condition 1; (b) $t = 50$, random initial condition 2; (c) $t = 78$, random initial condition 1; (d) $t = 78$, random initial condition 2.

that the magnitude of the vorticity for random initial condition 1 is a little larger than that for random initial condition 2. The contour plots correspond to the most unstable mode. Figures 12 and 13 show that it takes different times for the system to pick up the most unstable mode from different random initial conditions.

The streamwise velocity level surfaces of equal magnitudes but opposite signs for the perturbation at the critical wavenumber are given in figure 14. The dark and light parts of the graph in figure 14 correspond to large negative and positive streamwise velocity level surfaces, respectively. It is clear that the positive and negative velocity surfaces ‘twist’ together along the streamwise direction in a helical manner. Note that helical mode of disturbance is found to be the most unstable for Case II in Das & Arakeri (1998). The phase difference between the bottom and top vortices in their experiments was about 180° . In § 3.3, we shall use our model in an attempt to explain some of the experimental results obtained of Das & Arakeri (1998) for unsteady flows generated by the motion of a piston.

In all the four cases considered, Das & Arakeri (1998) observed that the instability was associated with the formation of a periodic array of vortices. It was found that

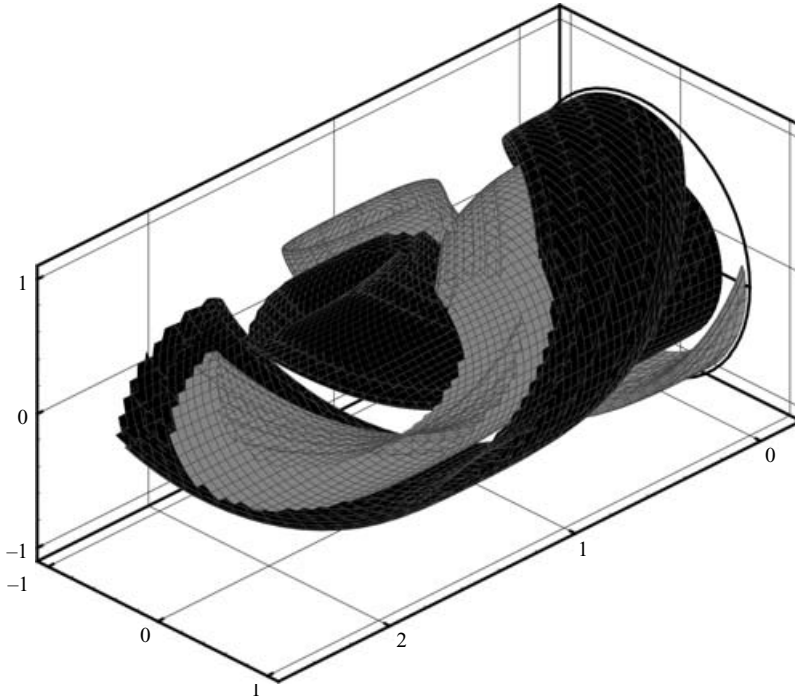


FIGURE 14. Level surface for the streamwise velocity perturbation for Case II ($\alpha = 2.65, n = 1$).

the spacing between the vortices, the time of their formation and their ‘fate’ depends on the experimental conditions. In particular, Das & Arakeri (1998) reported that there was no breakdown of vortices in Cases I and IV while in Cases II and III they observed vortex breakdown and rapid transition to turbulence. The evolution of energy growth is used here in an attempt to explain the different behaviours of vortices in the experiments. The procedure we used in the analysis was as follows. The energy growth for each case was calculated for the critical wavenumber which was found from the data in table 2. The initial conditions for $\hat{u}, \hat{v}, \hat{w}$ were specified as described before. For each of the four cases, the growth rates for two different random initial perturbations are shown in figure 18. The integral $\int_{t_p}^{t_s} G_E dt$ is calculated, where t_s is the time at which the growth rate becomes zero (in other words, at $t = t_s$ the perturbation stops growing), and t_p is obtained from the experimental observations of Das & Arakeri (1998). The magnitude of the integral is used in an attempt to decide whether vortex breakdown is possible. Note that using (15), we can easily show that the value of the integral is $\ln E(t_s) - \ln E(t_p) = \ln[E(t_s)/E(t_p)]$. In other words, the magnitude of the integral is directly related to energy amplification factor in the interval (t_p, t_s) .

The energy curves for Cases I to IV are plotted in figures 15(a) to 15(d), respectively. The hashed areas in these figures define the net gain in energy by the perturbations from time t_p to t_s . The calculations show that the net gains of kinetic energy by the perturbations from time t_p to t_s for Cases I, II, III and IV are 0.07, 4.7, 16.3 and 2.4 (see table 3). These values indicate that Case III has the highest potential for flow transition followed by Cases II, IV and I. This is consistent with the experimental findings of Das & Arakeri (1998) who reported that there was no breakdown of vortices in

Case	t_p	t_s	Area	
I	80	86	0.07	No turbulence
II	78	149	4.7	Turbulence
III	72	195	16.3	Turbulence
IV	47	87	2.4	No turbulence

TABLE 3. Integrals of positive growth rates after perceptible time.

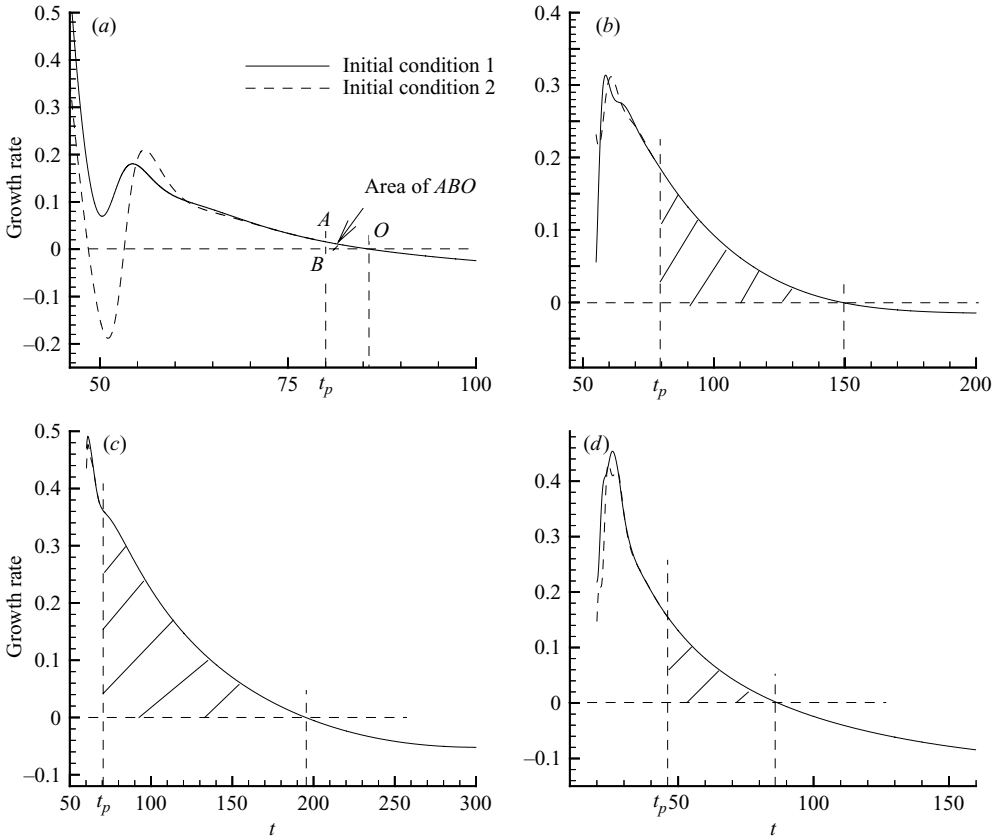


FIGURE 15. Growth rates of perturbations for decelerated flows (Das & Arakeri 1998). (a) Case I ($\alpha = 1.77, n = 1$), (b) Case II ($\alpha = 2.65, n = 1$), (c) Case III ($\alpha = 3.37, n = 1$), (d) Case IV ($\alpha = 5.50, n = 1$).

Cases I and IV whereas in Cases II and III they observed vortex breakdown and rapid transition to turbulence. It must be stressed that although transient growth constitutes a necessary condition for transition and the magnitude of this growth defines the likelihood of transition, a complete understanding of the transition from laminar to turbulent flows necessitates nonlinear analysis.

3.3. Quasi-steady assumption for transient decelerated flows

As has been shown earlier, linear stability analysis based on asymptotical growth for flows accelerated from rest totally fails to predict any perturbation growth and thus cannot be used to explain transition. However, it is found that for rapidly

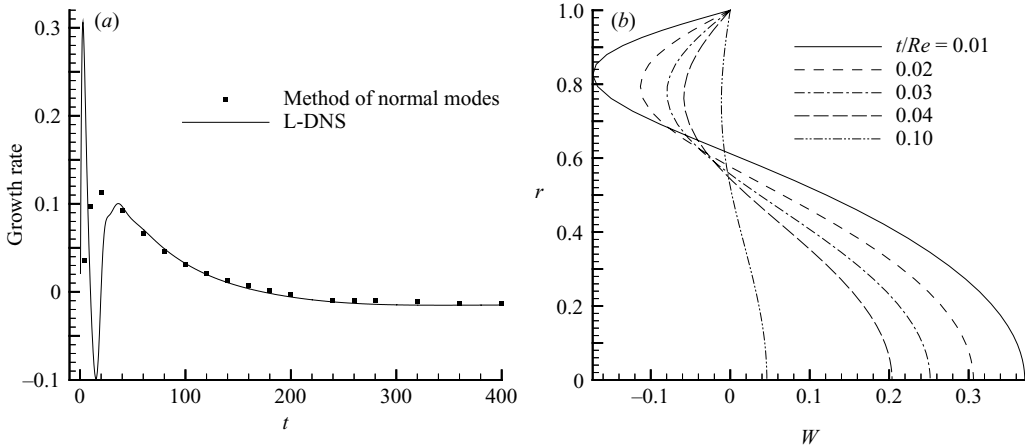


FIGURE 16. (a) Growth rates obtained from L-DNS and quasi-steady assumption and (b) velocity profiles for water hammer flow ($Re = 2000$, $\alpha = 1.5$, $n = 1$).

decelerated unsteady flows, large perturbation growth is associated with asymptotic energy growth. When the transition is not due to transient growth, the quasi-steady assumption might be used to predict the asymptotic growth rate. It is shown by Hall & Parker (1976) that the quasi-steady assumption works well asymptotically for large Reynolds numbers. In particular, Hall & Parker (1976) have shown that the difference between the growth rates with and without the quasi-steady assumption is of the order of $1/Re$. Here, L-DNS numerical calculations are performed in order to establish the limits of applicability of high-Reynolds-number theory. For a typical water hammer event where the steady flow is fully blocked by a valve closure, the initial velocity profile is instantaneously shifted by an amount which is equal to the mean of the undisturbed flow so that the mean flow after a pressure wave passage becomes zero. Examples of the velocity profiles corresponding to this case are plotted in figure 16(b). A vortex sheet is generated at the pipe wall and it starts to diffuse away from the pipe wall to the centreline. The asymptotic behaviour of perturbations is believed to be associated with the presence of the inflection point in the velocity profile. At the inflection point, where the velocity gradient has the maximum value, the perturbation velocity extracts energy from the base flow shear. This procedure provides energy for the perturbation. The rate of energy production depends on the velocity gradient. When the velocity gradient is changed, the rate of energy production also changes. This change possibly affects the growth rate of perturbation. If the change of base flow velocity gradient is slow compared with the growth rate of perturbation, then a quasi-steady assumption may be used since the calculated growth rates with and without the quasi-steady assumption will be close to each other.

This is illustrated in figure 16(a). In this figure, the growth rates for water hammer flow (3) with $Re = 2000$ at $\alpha = 1.5$, $n = 1$ are plotted. L-DNS calculations are shown by the solid lines and the dots represent the growth rates obtained with the quasi-steady assumption. For $t < 40$, the L-DNS results correspond to transient growth rate, which cannot be captured by the method of normal modes with the quasi-steady assumption. After $t > 40$, the agreement between the results from L-DNS and the method of normal modes is good. That is, asymptotic high-Reynolds-number theory works well for this case.

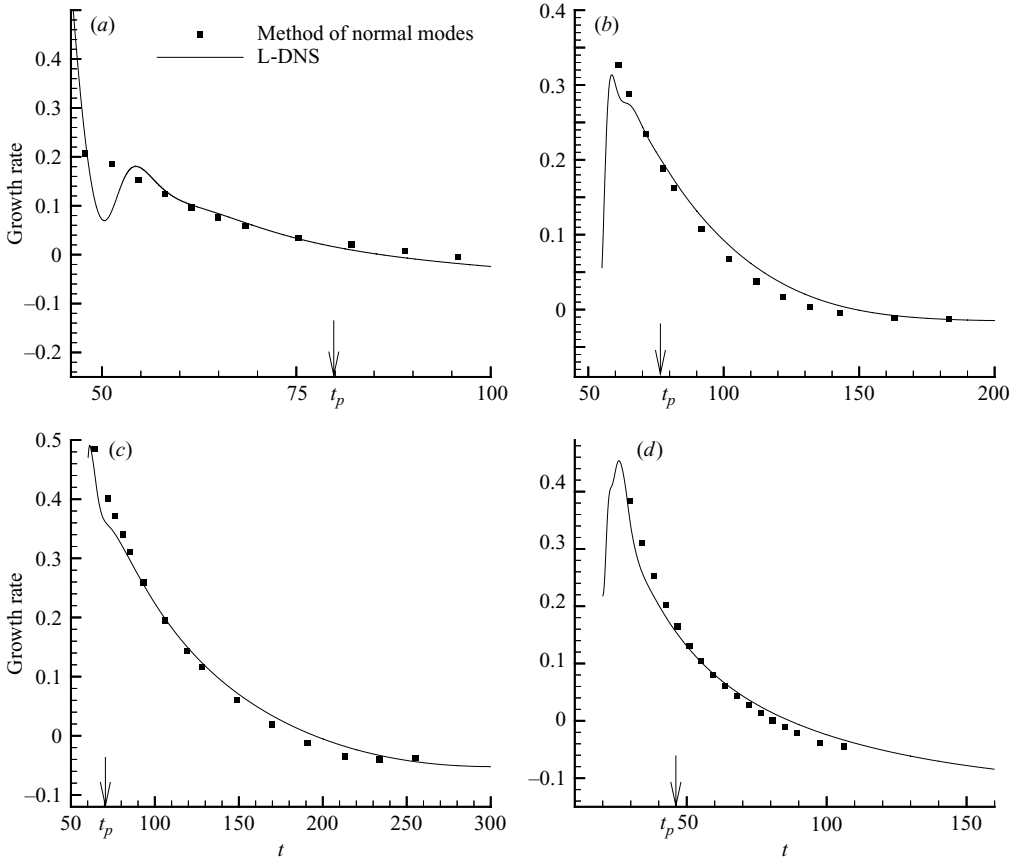


FIGURE 17. Growth rates obtained from L-DNS and method of normal modes for deceleration flows (Das & Arakeri 1998). (a) Case I ($\alpha = 1.77, n = 1$), (b) Case II ($\alpha = 2.65, n = 1$), (c) Case III ($\alpha = 3.37, n = 1$), (d) Case IV ($\alpha = 5.50, n = 1$).

The quasi-steady assumption for other transient flow cases, such as the experimental tests (Case I–Case IV) reported by Das & Arakeri (1998), is also studied. The growth rates obtained from L-DNS and the method of normal modes with the quasi-steady assumption are plotted in figure 17. The graphs show some disagreement between L-DNS and the method of normal modes in the initial stage, but the agreement between the results from two models is acceptable for larger times, specially after the time the perturbation is found to be perceptible in experiments. This supports the conclusion that the quasi-steady assumption is justified for the flow studied by Das & Arakeri (1998). Note that a characteristic feature of rapidly decelerated flows in Hall & Parker (1976) and Das & Arakeri (1998) is the presence of an inflection point in the velocity profile. It is well known that inflectional instability is important in the description of stability characteristics of steady flows. For truly unsteady flows, however, the instability associated with inflection points in the velocity profile may not be the only mechanism which affects the transition. On the other hand, different stability characteristics of accelerated flows (with no inflection points) and decelerated flows (with inflection points) discussed above show that an inflectional instability may play an important role also in unsteady flows.

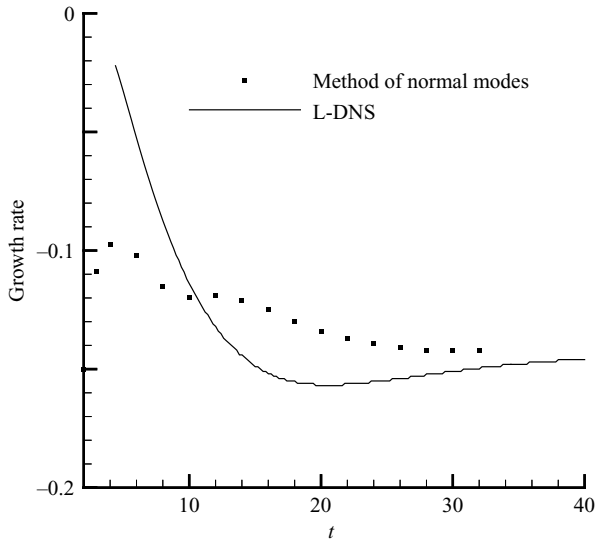


FIGURE 18. Growth rates obtained from L-DNS and quasi-steady assumption for water hammer flow ($Re = 200$, $\alpha = 1.8$, $n = 1$).

The growth rates for water hammer flow (3) with $Re = 200$ are plotted in figure 18. Obviously, the quasi-steady assumption is not good in this case. Note also that the values of Re in table 1 represent the magnitude of the Reynolds number in the beginning of the deceleration phase. During deceleration (see Hall & Parker 1976; Ghidaoui & Kolyshkin 2002) the critical values of Re decrease considerably and are of order 200 (as reported by Hall & Parker 1976 for the case of a planar channel) and of order 300 for Case I (as reported by Ghidaoui & Kolyshkin 2002). As a result, the quasi-steady assumption, which assumes that the base flow velocity is fixed, may not be justified in these cases. Therefore, although asymptotic theory predicts that the quasi-steady assumption is justified for large Reynolds numbers when the base flow is of an inflectional nature, transient growth analysis is required in order to define what would be considered as a ‘large Reynolds number’. For example, it is clear that Das & Arakeri (1998) and Ghidaoui & Kolyshkin (2002) erroneously considered a Reynolds number of the order of 200 to 300 to be large enough to justify the quasi-steady assumption for decelerating pipe flows.

4. Conclusions

The full temporal dynamics of linearized perturbations in unsteady rapidly accelerating and decelerating laminar flows in pipes is analysed in the present paper. Three types of unsteady base flows are considered: the flow accelerated from rest (Lefebvre & White 1989), the flow in a pipe–piston system which is generated by the controlled motion of the piston reported by Das & Arakeri (1998), and the water hammer flow which is obtained as a result of an instantaneous closure of the valve. The base flows in all three cases are unsteady and non-periodic.

Methods of linear stability theory are used to analyse the evolution of small perturbations in the fluid system. The Navier–Stokes equations are linearized in the neighbourhood of the base flow, Fourier decomposition is used in the azimuthal and longitudinal directions and the resulting system of partial differential equations

(where the independent variables are time and the radial coordinate) is solved as an initial-value problem. In contrast to the standard method of normal modes which is widely used in stability studies of steady laminar flows, the present approach allows us to trace the evolution of any small three-dimensional perturbation by specifying an arbitrary initial form of a perturbation. The energy growth function is used to analyse the temporal dynamics of perturbations.

The model is applied to the analysis of both short-time and long-time behaviour of the flow. It is found that during short-time transient growth, the initial conditions play an essential role in the development of instability. Uncorrelated random initial conditions are used in order to model perturbations which occur in the natural environment. The results for different samples are averaged and these averaged results are then compared with the experimental data of Lefebvre & White (1989) and Das & Arakeri (1998). The use of different random initial conditions and optimal initial conditions also shows that transient growth is not associated with a particular type of initial condition. The analysis of long-term asymptotics shows that for large times, the dependence of the growth rates on the initial condition disappears and different initial conditions give the same growth rates.

The results of numerical simulation for the case of flows accelerated from rest are compared with the experimental data in Lefebvre & White (1989). It is shown that transition cannot be explained by asymptotic growth – the growth rates for large time are all negative, indicating a linear stability of the flow. Hence, the method of normal modes in conjunction with the quasi-steady assumption will also fail to predict instability. However, perturbations experience large transient growth during short time after acceleration starts. The agreement between the time interval for which perturbations continue to grow and the time when instability is observed experimentally is good (the experimental transition time is found to be in the interval where perturbation energy increases substantially). However, computational results are obtained only for modes with fixed wavenumbers and, therefore, caution is needed when these results are compared with experimental data. On the other hand, calculations indicate that a transient growth mechanism may play an important role in the development of instability for flows accelerated from rest.

Numerical results are also compared with experimental findings reported by Das & Arakeri (1998). Using time \tilde{t}_p , when a perceptible wave appeared in the experiments, as the critical time for the instability to set in, we determined the critical wavenumber as the average (over several samples) of the wavenumbers at which the maximum growth is obtained at time $\tilde{t} = \tilde{t}_p$. This critical wavenumber is then used to evaluate the wavelength of the most unstable mode. Reasonable agreement is found between theoretical estimates and experimental data. An attempt is made to use the evolution of energy growth to explain why, in some cases, primary vortices (the result of primary instability) break down, but in other cases there is no breakdown. Das & Arakeri (1998) observed transition to turbulence in their experiments in two cases out of four. Using the model predictions, we calculated the integral of the growth rate over the time interval (t_p, t_s) , where t_s is the (dimensionless) time at which the growth rate becomes equal to zero. It is shown that if the integral is large enough, the flow had sufficient time for the perturbation to develop and as a result, vortex breakdown was observed.

The results of simulation are also used to analyse the structure of a perturbation. Analysis of vorticity contours for different initial conditions shows that a certain time is required for the perturbation to form a more or less organized structure. It is found that the structure of the most unstable perturbation is consistent with the observations of Das & Arakeri (1998).

The quasi-steady assumption, which is widely used in stability studies of unsteady laminar non-periodic flow, is analysed. The idea behind the quasi-steady assumption is that the base flow velocity profiles are assumed to be ‘frozen’ in time so that the stability characteristics are calculated for a fixed velocity profile where time, which the base flow depends on, is considered as a parameter. The analysis of the validity of the quasi-steady assumption is performed for four experimental cases reported by Das & Arakeri (1998). It is found that in all four cases the agreement between the calculated growth rates with and without the quasi-steady assumption is satisfactory. However, the accuracy of the quasi-steady assumption is better for higher Reynolds numbers.

Optimal perturbations are also considered for all three types of flow investigated here. The optimal growth curves show the upper limit of the energy growth and, therefore, can be used to assess the possibility of the bypass transition scenario. The results presented above show that the qualitative behaviour of optimal growth curves is similar to the behaviour of the growth curves for arbitrary initial conditions. However, the magnitude of the optimal growth is found to be considerably larger than the corresponding magnitudes for the initial conditions studied in the paper. This agrees with the numerical results of Criminale *et al.* (1997) where it is shown that the calculated transient growth for arbitrary initial conditions for two-dimensional perturbations in plane Poiseuille flow is found to be about 25 % of the optimal.

We wish to thank the Research Grant Council of Hong Kong for financial support under projects HKUST6179/02E and HKUST6113/03E.

REFERENCES

- BEN-DOV, G., LEVINSKI, V. & COHEN, J. 2003 On the mechanism of optimal disturbances: the role of a pair of nearly parallel modes. *Phys. Fluids* **15**, 1961–1972.
- BERGSTRÖM, L. 1992 Initial algebraic growth of small angular dependent disturbances in pipe Poiseuille flow. *Stud. Appl. Maths* **87**, 61–79.
- BERGSTRÖM, L. 1993 Optimal growth of small disturbances in pipe Poiseuille flow. *Phys. Fluids A* **5**, 2710–2720.
- BRUNONE, B., KARNEY, B., MECARELLI, M. & FERRANTE, M. 2000 Velocity profiles and unsteady pipe friction in transient flow. *J. Water Resources Planning and Management*, ASCE **126**, 236–244.
- BUTLER, K. M. & FARRELL, B. F. 1992 Three-dimensional optimal perturbations in viscous shear flow. *Phys. Fluids A* **4**(8), 1637–1650.
- CHEN C. F. & KIRCHNER, R. P. 1971 Stability of time-dependent rotational Couette flow. Part 2. Stability analysis. *J. Fluid Mech.* **48**, 365–384.
- CORBETT, P. & BOTTARO, A. 2000 Optimal perturbations for boundary layers subject to streamwise pressure gradient. *Phys. Fluids* **12**, 120–130.
- CRIMINALE, W. O., JACKSON, T. L., LASSEIGNE, D. G. & JOSLIN, R. D. 1997 Perturbation dynamics in viscous channel flows. *J. Fluid Mech.* **339**, 55–75.
- DAS, D. & ARAKERI, J. H. 1998 Transition of unsteady velocity profiles with reverse flow. *J. Fluid Mech.* **374**, 251–283.
- ELLINGSEN, T. & PALM, E. 1975 Stability of linear flow. *Phys. Fluids* **18**(4), 487–488.
- GHIDAOU, M. S. & KOLYSHKIN, A. A. 2001 Stability analysis of velocity profiles in water-hammer flows. *J. Hydraul. Engng* ASCE **127**, 499–512.
- GHIDAOU, M. S. & KOLYSHKIN, A. A. 2002 A quasi-steady approach to the instability of time-dependent flows in pipes. *J. Fluid Mech.* **465**, 301–330.
- GREENBLATT, D. & MOSS, E. A. 2003 Rapid transition to turbulence in pipe flows accelerated from rest. *J. Fluids Engng* **125**, 1072–1075.
- GROMEKA, I. S. 1882 On the theory of fluid motion in narrow cylindrical pipes. *Kazan University Research Notes*, 32 pp. (In Russian).

- HALL, P. 1975 The stability of Poiseuille flow modulated at high frequencies. *Proc. R. Soc. Lond. A* **465**, 453–464.
- HALL, P. & PARKER, K. H. 1976 The stability of the decaying flow in a suddenly blocked channel flow. *J. Fluid Mech.* **75**, 305–314.
- HENNINGSON, D. S. & REDDY, S. C. 1994 On the role of linear mechanisms in transition to turbulence. *Phys. Fluids* **6**(3), 1396–1398.
- HINO, M., SAWAMOTO, M. & TAKASU, S. 1976 Experiments on transition to turbulence in an oscillatory pipe flow. *J. Fluid Mech.* **75**, 193–207.
- JOSEPH, D. D. 1976 *Stability of Fluid Motion I*. Springer.
- VON KERCZEK, C. 1982 The stability of oscillatory plane Poiseuille flow. *J. Fluid Mech.* **116**, 91–114.
- LANDAHL, M. T. 1980 A note on an algebraic instability of inviscid parallel shear flows. *J. Fluid Mech.* **98**, 243–251.
- LASSEIGNE, D. G., JOSLIN, R. D., JACKSON, T. L. & CRIMINALE, W. O. 1999 The transient period for boundary layer disturbances. *J. Fluid Mech.* **381**, 89–119.
- LEFEBVRE, P. J. & WHITE, F. M. 1989 Experiments on transition to turbulence in a constant-acceleration pipe flow. *J. Fluids Engng* **124**, 236–240.
- LEVIN, O. & HENNINGSON, D. S. 2003 Exponential vs algebraic growth and transition prediction in boundary layer flow. *Flow Turbulence Combust.* **70**, 183–210.
- LOPEZ, J. M., MARQUES, F. & SHEN, J. 2002 An efficient spectral-projection method for the Navier–Stokes equations in cylindrical geometries II. Three-dimensional cases. *J. Comput. Phys.* **176**, 384–401.
- MOIN, P. & KIM, J. 1980 On the numerical solution of time-dependent viscous incompressible fluid flows involving solid boundaries. *J. Comput. Phys.* **35**, 381–392.
- REDDY, S. C. & HENNINGSON, D. S. 1993 Energy growth in viscous channel flows. *J. Fluid Mech.* **252**, 209–238.
- SCHLICHTING, H. 1979 *Boundary-Layer Theory*. McGraw–Hill.
- SCHMID, P. J. 2000 Linear stability theory and bypass transition in shear flows. *Phys. Plasmas* **7**, 1788–1794.
- SCHMID, P. J. & HENNINGSON, D. S. 1994 Optimal energy density growth in Hagen–Poiseuille flow. *J. Fluid Mech.* **277**, 195–225.
- SCHMID, P. J. & HENNINGSON, D. S. 2001 *Stability and Transition in Shear Flows*. Springer.
- SZYMANSKI, P. 1932 Some exact solutions of the hydrodynamic equations of a viscous fluid in the case of a cylindrical tube. *J. Math. Pures Appl.* **11**, 67–107.
- VANDERPLAATS RESEARCH & DEVELOPMENT 2000 *DOT Manual*. Colorado.
- WATERS, S. L. & PEDLEY, T. J. 1999 Oscillatory flow in a tube of time-dependent curvature. Part 1. Perturbation to flow in a stationary curved tube. *J. Fluid Mech.* **383**, 327–352.
- WYLIE, E. B. & STREETER, V. L. 1993 *Fluid Transient in Systems*, Prentice–Hall.
- YANG, W. H. & YIH, C. S. 1977 Stability of time-periodic flows in a circular pipe. *J. Fluid Mech.* **82**, 497–505.
- ZHAO, M., GHIDAOU, M. S. & KOLYSHKIN, A. A. 2004 Investigation of the mechanisms responsible for the breakdown of axisymmetry in pipe transient. *J. Hydraul. Res.* **42**, 645–656.